The NEDD8-activating enzyme inhibitor MLN4924 reduces ischemic brain injury in mice

Huilin Yu[a,1], Haiyu Luo[a,1], Luping Chang[a,1], Shisheng Wang[b,1], Xue Geng[a], Lijing Kang[a], Yi Zhong[b], Yongliang Cao[a], Ranran Wang[a], Xing Yang[a], Yuanbo Zhu[a], Mei-Juan Shi[a], Yue Hu[a], Zhongwang Liu[a], Xuhui Yin[c], Yunwei Ran[c], Hao Yang[b,2], Wenying Fan[a,2], and Bing-Qiao Zhao[a,2]

[a]Department of Translational Neuroscience, Jing'an District Centre Hospital of Shanghai, State Key Laboratory of Medical Neurobiology and MOE Frontiers Center for Brain Science, Institutes of Brain Science, Fudan University, Shanghai 200032, China; [b]Institutes for Systems Genetics and NHC Key Lab of Transplant Engineering and Immunology, Sichuan Provincial Engineering Laboratory of Pathology in Clinical Application, West China Hospital, Sichuan University, Chengdu 610041, China; and [c]Institute of Neuroscience and Third Affiliated Hospital, Zhengzhou University, Zhengzhou 450052, China

Edited by Lawrence Steinman, Departments of Neurology and Neurological Sciences and Pediatrics, Stanford University, Stanford, CA; received June 28, 2021; accepted December 14, 2021

Blood–brain barrier (BBB) breakdown and inflammation occurring at the BBB have a key, mainly a deleterious role in the pathophysiology of ischemic stroke. Neddylation is a ubiquitylation-like pathway that is critical in various cellular functions by conjugating neuronal precursor cell-expressed developmentally down-regulated protein 8 (NEDD8) to target proteins. However, the roles of neddylation pathway in ischemic stroke remain elusive. Here, we report that NEDD8 conjugation increased during acute phase after ischemic stroke and was present in intravascular and intraparenchymal neutrophils. Inhibition of neddylation by MLN4924, also known as pevonedistat, inactivated cullin-RING E3 ligase (CRL), and reduced brain infarction and improved functional outcomes. MLN4924 treatment induced the accumulation of the CRL substrate neurofibromatosis 1 (NF1). By using virus-mediated NF1 silencing, we show that NF1 knockdown abolished MLN4924-dependent inhibition of neutrophil trafficking. These effects were mediated through activation of endothelial P-selectin and intercellular adhesion molecule-1 (ICAM-1), and blocking antibodies against P-selectin or anti–ICAM-1 antibodies reversed NF1 silencing-induced increase in neutrophil infiltration in MLN4924-treated mice. Furthermore, we found that NF1 silencing blocked MLN4924-afforded BBB protection and neuroprotection through activation of protein kinase C δ (PKCδ), myristoylated alanine-rich C-kinase substrate (MARCKS), and myosin light chain (MLC) in cerebral microvessels after ischemic stroke, and treatment of mice with the PKCδ inhibitor rottlerin reduced this increased BBB permeability. Our study demonstrated that increased neddylation promoted neutrophil trafficking and thus exacerbated injury of the BBB and stroke outcomes. We suggest that the neddylation inhibition may be beneficial in ischemic stroke.

ischemic stroke | neddylation | MLN4924 | neutrophil trafficking | blood–brain barrier breakdown

Stroke continues to be a leading cause of death and the most frequent cause of disability in adults. Despite significant advances in decoding the pathophysiology of cerebral ischemia, therapeutic options for stroke are still limited. Ischemic injury to the brain rapidly triggers adhesion molecule expression on the activated endothelium (1), resulting in rolling, adhesion, and extravasation of blood-derived inflammatory cells (2). Infiltrating inflammatory cells, including neutrophils, result in irreversible impairment of blood–brain barrier (BBB) function and tissue damage through the release of reactive oxygen species (ROS), proteolytic enzymes, and proinflammatory mediators (3). However, our understanding of the links between BBB breakdown and peripheral neutrophils infiltrating the ischemic brain is still incomplete.

Neddylation is the process of posttranslational protein modification by conjugating the ubiquitin-like protein, neuronal precursor cell-expressed developmentally down-regulated protein 8 (NEDD8), to target proteins (4). This process is catalyzed by NEDD8-activating enzyme E1 (NAE1 and UBA3), NEDD8-conjugating enzyme E2 (UBC12), and NEDD8 E3 ligase (5). The best characterized substrates of NEDD8 are cullins (6), which are scaffold proteins for the cullin-RING E3 ligase (CRL) (7). The conjugation of NEDD8 to cullins leads to the activation of CRL (8), which ubiquitinates a multitude of different proteins for targeted degradation (9). Recently, the neddylation pathway was reported to contribute to growth of a variety of cancer cells and inflammatory responses (10). In contrast, inhibition of neddylation by MLN4924, which is a small molecule inhibitor of NAE, suppressed tumor growth, reduced inflammation, and prevented atherogenesis (11–13). However, to the best of our knowledge, the role of neddylation in ischemic stroke has not been addressed so far.

Using a mouse model of focal transient cerebral ischemia, we show that neddylation was up-regulated in the peri-infarct cortex after stroke and was expressed in neutrophils. Treatment with the neddylation inhibitor MLN4924 reduced brain infarction and improved neurological functions. We also demonstrated

Significance

Ischemic stroke is a leading cause of death and disability with limited therapies. Neuronal precursor cell-expressed developmentally downregulated protein 8 (NEDD8) is a ubiquitin-like protein that is involved in protein neddylation. The first-in-class anticancer agent called MLN4924 plays a crucial role in suppressing tumorigenesis and attenuating inflammatory responses due to specifically inhibiting NEDD8-activating enzyme. Here, we investigated the potential protective role of MLN4924 after experimental stroke. We showed that the neddylation pathway is overactivated in the brain following cerebral ischemia. Inhibition of neddylation by MLN4924 protects the brain against ischemic injury by attenuating neutrophil extravasation and maintaining blood–brain barrier integrity. Our findings provide insights into the promising treatment with neddylation inhibition for ischemic brain injury.

Author contributions: H. Yu, H. Yang, W.F., and B.Z. designed research; H. Yu, H.L., L.C., S.W., X.G., L.K., Y.Z., Y.C., R.W., X. Yang, Y.Z., M.S., Y.H., Z.L., X. Yin, and Y.R. performed research; H. Yu, H.L., L.C., and S.W. analyzed data; and H. Yu, H. Yang, W.F., and B.Z. wrote the paper.

The authors declare no competing interest.

This article is a PNAS Direct Submission.

[1]H. Yu, H.L., L.C., and S.W. contributed equally to this work.

[2]To whom correspondence may be addressed. Email: bingqiaoz@fudan.edu.cn, wenyingf@fudan.edu.cn, or yanghao@scu.edu.cn.

This article contains supporting information online at http://www.pnas.org/lookup/suppl/doi:10.1073/pnas.2111896119/-/DCSupplemental.

Published January 31, 2022.

that MLN4924-afforded neuroprotection was mediated via anti-inflammatory and BBB-protective effects involving the accumulation of CRL substrate neurofibromatosis 1 (NF1).

Results

Neddylation Pathway Is Activated in the Brain after Ischemic Stroke. To explore the function of the neddylation pathway in ischemic stroke, we subjected mice to 1-h transient focal cerebral ischemia and examined brains at 3, 6, 12, and 24 h. We found that the global protein neddylation in brain lysates were increased 3 h poststroke, reached a peak around 12 h, and continued over 24 h (Fig. 1 *A* and *B*). Using a specific NEDD8 antibody that recognizes NEDD8-conjugated proteins, we confirmed that NEDD8 was up-regulated in the peri-infarct cortex at 12 and 24 h after stroke compared to sham-operated brains (Fig. 1*C*). In the ischemic cortex, NEDD8 was expressed in $Ly6G^+$ neutrophils inside the blood vessels and parenchyma (Fig. 1*D*), suggesting that NEDD8 may play a role in neutrophil extravasation from blood vessels and consequent BBB impairment after ischemia. In addition, we noted colocalization of NEDD8 with $CD31^+$ endothelial cells and $Iba1^+$ microglia cells but only a little NEDD8 staining in $GFAP^+$ astrocytes, $F4/80^+$ monocytes/macrophages, and $NeuN^+$ neurons (Fig. 1*D*). The increased protein level of NEDD8 was accompanied by up-regulation of the NEDD8-activating enzyme E1-NAE subunits (NAE1 and UBA3) and NEDD8-conjugating enzyme E2 (UBC12) at 6 to 24 h after stroke (Fig. 1 *E*–*H*). The best characterized substrates of neddylation are cullin-family proteins (6). Therefore, we asked whether cullin neddylation might change after stroke. We observed a marked increase in NEDD8-cullin-1 conjugation at 12 and 24 h in the ischemic cortex (Fig. 1 *E* and *I*). Taken together, these data indicate that ischemic stroke induced protein neddylation. However, we found that there was no significant difference in mRNA levels of NEDD8, NAE1, UBA3, and UBC12 between sham-operated mice and mice that underwent middle cerebral artery (MCA) occlusion (*SI Appendix*, Fig. S1 *A*–*D*), suggesting that ischemic stroke does not influence the transcriptional properties of the NEDD8 pathway.

Inhibition of Neddylation by MLN4924 Reduces Brain Damage after Ischemic Stroke. To address whether neddylation plays an active role in ischemic stroke, we inhibited the neddylation pathway by the specific NAE inhibitor MLN4924 (14). Treatment with MLN4924 significantly reduced cullin-1 neddylation (Fig. 2 *A* and *B*), showing the inactivation of CRL. Previous studies have shown that proteotoxic stress induced an increase in the protein neddylation, which occurred through the ubiquitin E1 enzyme Ube1-dependent mechanism (15). We therefore measured the effect of Ubiquitin E1 on NEDD8 conjugation by silencing the ubiquitin E1 enzyme UBE1 (UAE/UBA1). We confirmed that UBE1 silencing by adenoviral short hairpin RNA (shRNA) administration into the brain of mice resulted in a significant decrease in UBE1 expression at 12 and 24 h after stroke (Fig. 2 *C* and *D*). We then observed that shRNA silencing of UBE1 had no effect on the level of NEDD8 conjugation (Fig. 2 *C* and *E*). However, when mice were treated with MLN4924, the NEDD8 neddylation was significantly decreased (Fig. 2 *F* and *G*). These results suggest that the increase in stroke-meditated neddylation may occur through the canonical NEDD8 enzyme NAE. Compared with the vehicle controls, injection of MLN4924 resulted in a 43.8% reduction of infarct volume at 24 h after stroke (Fig. 2 *H* and *I*). MLN4924-treated mice had significant improvements in functional outcomes, as shown by forelimb force and rotarod latency (Fig. 2 *J* and *K*).

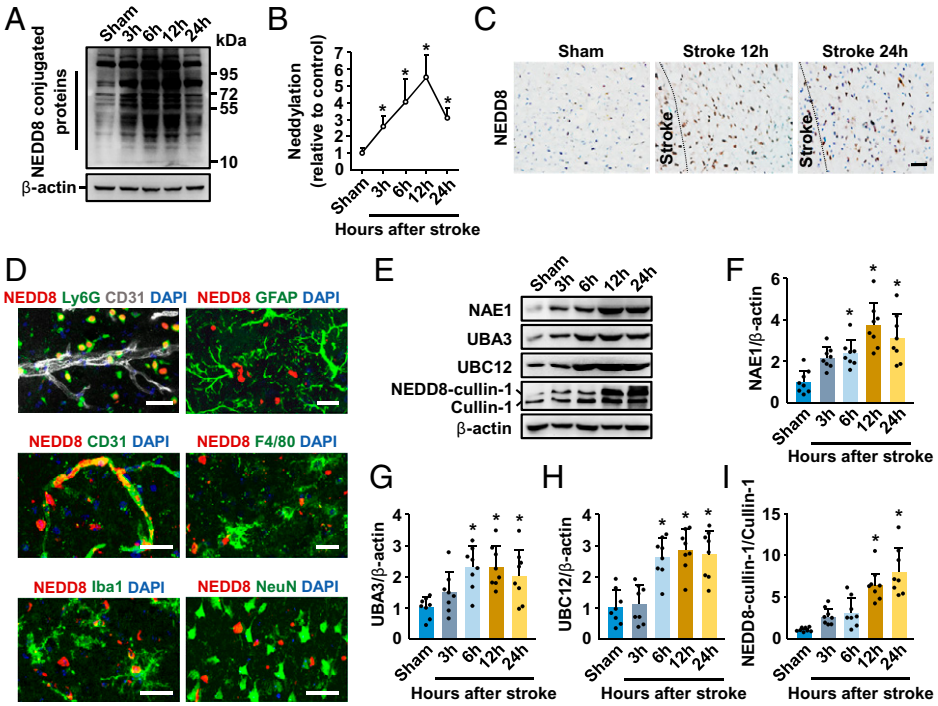

Fig. 1. Neddylation pathway is up-regulated after ischemic stroke. (*A*) Western blot assay for global NEDD8 conjugation in the ipsilateral hemisphere in sham-operated mice and ischemic mice 3, 6, 12, and 24 h following operation. (*B*) Quantitative determinations of global NEDD8 conjugation for each group ($n = 8$). (*C*) Representative NEDD8 immunostaining at 12 and 24 h after stroke compared with sham-operated mice. (Scale bar, 50 μm.) (*D*) Double immunostaining of NEDD8 (red) with neutrophils (Ly6G), endothelial cells (CD31), microglial cells (Iba1), astrocytes (GFAP), monocytes/macrophages (F4/80), and neurons (NeuN) in mice subjected to ischemic stroke. In the *Upper Left*, white indicates CD31-positive microvessels. Nuclei were stained with DAPI (blue). (Scale bar, 40 μm.) (*E*) Western blot assay for NAE1, UBA3, UBC12, and cullin-1 neddylation in sham-operated mice and ischemic mice 3, 6, 12, and 24 h following operation. (*F*–*I*) Quantitative determinations of NAE1, UBA3, UBC12, and cullin-1 neddylation for each group ($n = 8$). Data were analyzed using one-way ANOVA followed by Bonferroni multiple comparison test. Values are mean ± SD. $^*P < 0.05$.

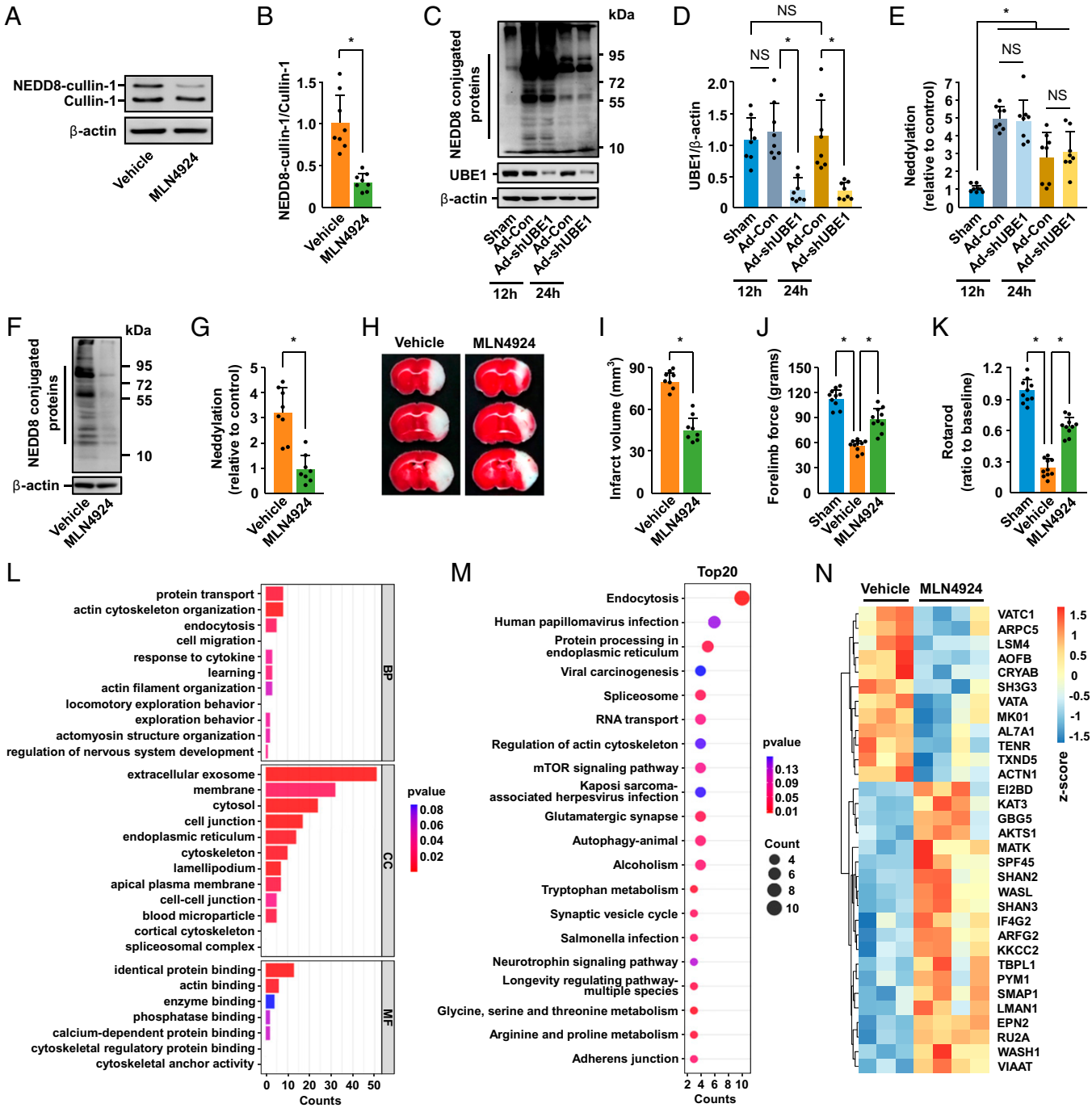

Fig. 2. MLN4924 reduces ischemic cerebral injury and improves behavioral outcomes. (*A*) Inhibition of cullin-1 neddylation by MLN4924. Immunoblotting of lysates from the ipsilateral hemisphere in ischemic mice treated with vehicle or MLN4924 24 h after stroke. (*B*) Quantitative determinations of cullin-1 neddylation for each group ($n = 8$). (*C*) Western blot assay for NEDD8 conjugation and UBE1 levels in the ipsilateral hemisphere in ischemic mice treated with control adenovirus (Ad-Con) or UBE1 shRNA (Ad-shUBE1) 12 and 24 h following stroke. (*D* and *E*) Quantitative determinations of UBE1 levels and NEDD8 conjugation for each group ($n = 8$). (*F* and *G*) Representative Western blot and quantification of NEDD8 conjugation in the ipsilateral hemisphere in ischemic mice treated with vehicle or MLN4924 24 h following stroke ($n = 8$). (*H*) Representative photographs of 2,3,5-triphenyl tetrazolium chloride–stained coronal brain sections showing smaller cerebral infarct in mice treated with MLN4924 than in mice treated with vehicle 24 h after stroke. (*I*) Quantitation of infarct volumes for each group ($n = 8$). (*J* and *K*) MLN4924 improved behavioral outcomes in forelimb force test and rotarod test ($n = 10$). (*L*) Brain proteomics characterization by high-performance liquid chromatography-tandem mass spectrometry in ischemic mice treated with vehicle or MLN4924. Gene Ontology analysis showed that differentially expressed proteins were significantly enriched in biological processes (BP), cell components (CC), and molecular functions (MF). (*M*) The top 20 pathways based on KEGG enrichment analysis. (*N*) Heatmap showing the key differential proteins enriched in the top 20 pathways. Data were analyzed using unpaired Student's *t* test or one-way ANOVA followed by Bonferroni multiple comparison test. Values are mean ± SD. $^*P < 0.05$. NS, not significant.

To investigate protein expression differences in the ischemic brain between mice treated with vehicle and MLN4924, high-throughput quantitative proteomics based on high-performance liquid chromatography-tandem mass spectrometry was performed. Gene Ontology analysis depicted that differentially expressed proteins were markedly enriched in actin cytoskeleton

organization, endocytosis, actin filament organization, cell migration, and cell junction (Fig. 2*L*). Kyoto Encyclopedia of Genes and Genomes (KEGG) analysis revealed the top 20 KEGG-annotated pathways derived from the differentially expressed proteins upon MLN4924 treatment (Fig. 2*M*). Among them include pathways involved in the regulation of endoplasmic reticulum, spliceosome, RNA transport, actin cytoskeleton, and adherens junction. In addition, the KEGG-enriched pathways associated with the control of endocytosis, glutamatergic synapse, autophagy, glycine, serine and threonine metabolism, and arginine and proline metabolism have been reported to be involved in the pathogenesis of stroke (16–21). For the aforementioned 20 major KEGG pathways, the key differential proteins are shown in Fig. 2*N*. A file containing identified proteins is provided in Dataset S1. In future, further investigation of the downstream signaling pathways involved in neddylation triggering inhibition will be essential.

MLN4924 Blunts BBB Damage after Ischemic Stroke. Increase in BBB permeability greatly influenced the outcome of stroke (22). To investigate the role of MLN4924 on BBB permeability, we first analyzed Evans blue dye extravasation at 24 h after MCA occlusion (MCAO). This experiment showed that there was a large decrease in BBB permeability in the ischemic brain in MLN4924-treated animals compared with vehicle-treated mice (Fig. 3 *A* and *B*). Using in vivo multiphoton microscopy of intravenously injected fluorescein isothiocyanate (FITC)–dextran, we found an intact BBB in sham-operated mice and an increased BBB permeability to fluorescent dextran in mice subjected to stroke (Fig. 3 *C* and *D*). Treatment with MLN4924 significantly reduced BBB damage at 24 and 48 h compared with vehicle-treated animals. Similarly, mice treated with MLN4924 exhibited a substantial reduction in the extravasation of injected fluorescent bovine serum albumin (BSA) (Fig. 3 *E* and *F*). We next studied leakage of IgG, an endogenous blood-derived protein, in the brain. Western blot analysis of IgG in vascular-depleted brain homogenates revealed that MLN4924-treated mice had a 48.8% reduction in IgG accumulation in the brain parenchyma compared with vehicle-treated mice (Fig. 3 *G* and *H*). Immunostaining for IgG and the endothelial cell marker CD31 further

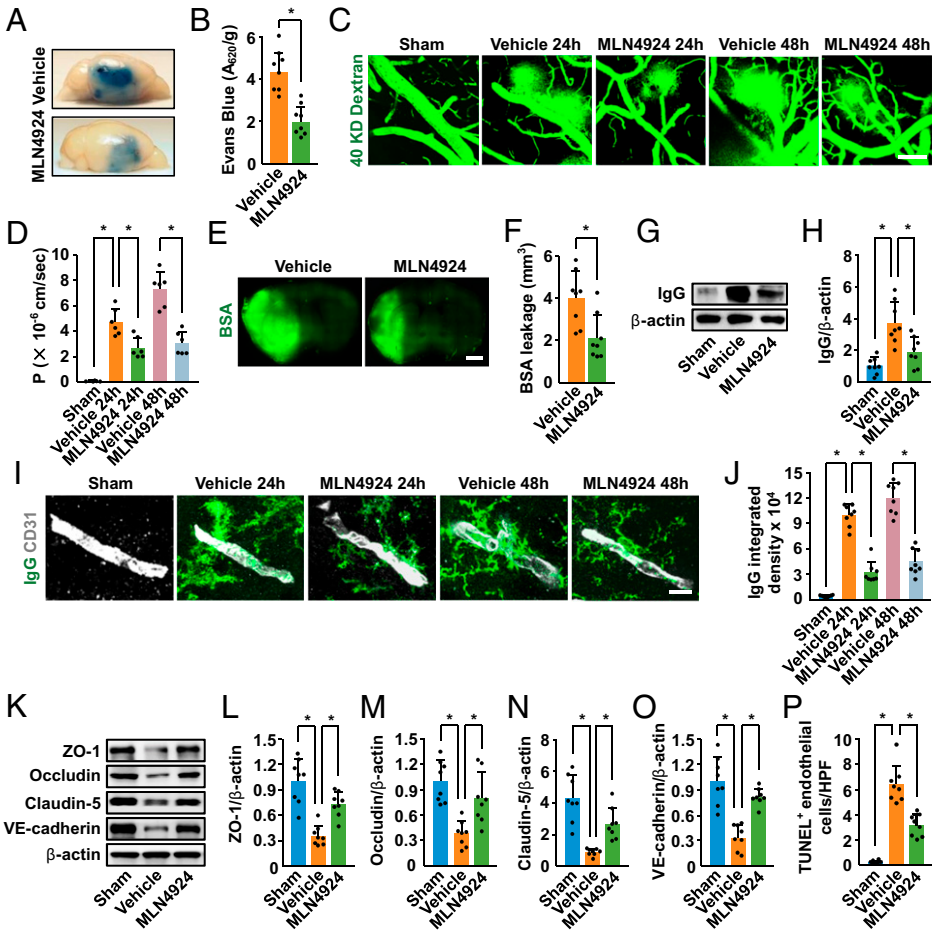

Fig. 3. MLN4924 attenuates BBB breakdown after ischemic stroke. (*A* and *B*) Representative images and quantification of Evans blue extravasation 24 h after stroke in mice treated with vehicle or MLN4924 ($n = 8$). (*C*) Representative in vivo multiphoton microscopic images of intravenously injected FITC-dextran (MW = 40 KDa) leakage from cortical vessels in sham-operated mice and ischemic mice treated with vehicle or MLN4924 24 and 48 h after stroke. (Scale bar, 100 μm.) (*D*) Quantification of the permeability (P) product of FITC-dextran for each group ($n = 6$). (*E*) Representative images of coronal brain sections showing the leakage of intravenously injected BSA into the brain. (Scale bar, 1 mm.) (*F*) Quantification of extravascular BSA fluorescence ($n = 8$). (*G*) Western blot assay for IgG levels in capillary-depleted brain tissue. (*H*) Quantification of IgG deposits in capillary-depleted brain tissue ($n = 8$). (*I*) Representative images and quantitation of IgG perivascular accumulation (green) in sham-operated mice and ischemic mice treated with vehicle or MLN4924 24 and 48 h after stroke. Capillaries were stained with CD31 (white). (Scale bar, 10 μm.) (*J*) Quantitation of IgG perivascular accumulation ($n = 8$). (*K*–*O*) Reduced tight junction protein ZO-1, occludin, and claudin-5 and adherens junction protein VE-cadherin levels in isolated brain microvessels of ischemic mice and reversal by MLN4924 treatment ($n = 8$). (*P*) Immunohistochemical quantification of TUNEL-positive endothelial cells in sham-operated mice and ischemic mice treated with vehicle or MLN4924 24 h after stroke ($n = 8$). Data were analyzed using unpaired Student's *t* test or one-way ANOVA followed by Bonferroni multiple comparison test. Values are mean ± SD. $^*P < 0.05$. HPF, high-power field.

confirmed great reduction in perivascular IgG deposits at 24 and 48 h in MLN4924-treated mice (Fig. 3 *I* and *J*).

The permeability of BBB is impeded by endothelial junctions, which are reduced in stroke leading to the BBB breakdown (22). We studied whether the expression of the BBB junctional proteins is altered by MLN4924 treatment in the ischemic brain. Immunoblotting of isolated brain microvessels showed that the loss of tight junction proteins ZO-1, occludin, and claudin-5 as well as the adherens junction protein VE-cadherin caused by ischemia was abolished by MLN4924 treatment (Fig. 3 *K*–*O*), suggesting that MLN4924 may play an important role in the maintenance of vascular integrity. We next asked whether MLN4924 could reduce ischemic endothelial injury. Immunohistochemical quantification showed that TUNEL-positive endothelial cells were significantly suppressed in MLN4924-treated brains compared to vehicle controls (Fig. 3*P* and *SI Appendix*, Fig. S2*A*). This finding is consistent with the report showing that MLN4924 treatment decreased liver fibrosis-induced apoptosis (10).

MLN4924 Reduces Cerebral Neutrophil Invasion and Proinflammatory Cytokine Production. Based on these findings, we searched to elucidate the underlying cause for the protective effect of MLN4924 on BBB breakdown. Because we showed that NEDD8 is expressed in neutrophils (Fig. 1*D*) inside the blood vessels, we determined the effect of MLN4924 on neutrophil invasion. In vivo multiphoton microscopy analysis of intravenously injected PE-Ly6G showed that neutrophils adhered to the microvascular endothelium and migrated into the injured brain in mice subjected to stroke (Fig. 4*B*), whereas neutrophils rarely adhered or extravasated in sham-operated mice. We observed that the number of adherent neutrophils and extravasation of neutrophils from blood vessels into the brain parenchyma at 12 h after stroke were both substantially reduced in MLN4924-treated mice compared with vehicle-treated mice (Fig. 4 *C* and *D*). We also found that the neutrophil rolling velocity was significantly increased in mice injected with MLN4924 (Fig. 4*E*).

Consistent with these observations, immunohistochemical quantification revealed significantly decreased numbers of neutrophils in the ischemic hemispheres at 12, 24, and 48 h after ischemic stroke in mice treated with MLN4924 (Fig. 4*F* and *SI Appendix*, Fig. S3*A*). These results were further confirmed by Western blot using an anti-Ly6G antibody (Fig. 4*G*). Significantly lower amount of neutrophil was observed in the ischemic brains in mice treated with MLN4924 (Fig. 4*H*). Quantification of the neutrophil-specific enzyme myeloperoxidase (MPO)

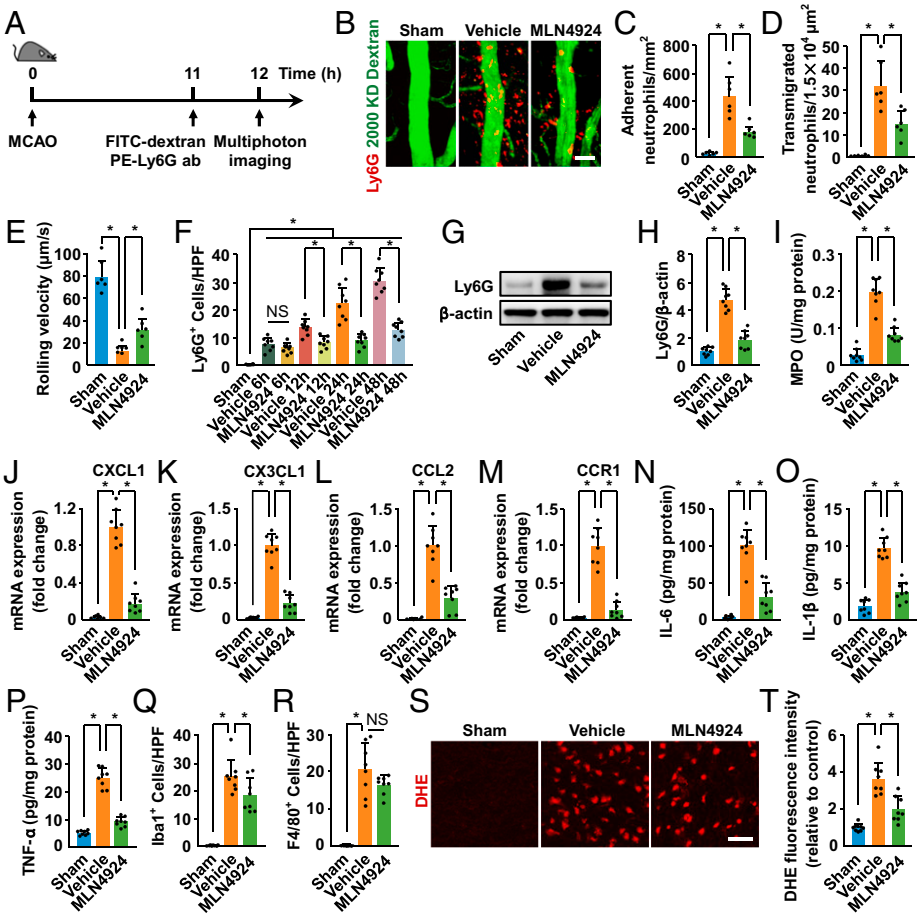

Fig. 4. MLN4924 reduces neutrophil infiltration and proinflammatory cytokines expression in the ischemic brains. (*A*) Timeline of multiphoton microscopic experiments. (*B*) Representative in vivo multiphoton microscopic images of rolling and adherent neutrophils (red) inside the blood vessels (green) and of infiltrated neutrophils into the brain parenchyma. (Scale bar, 40 μm.) (*C*–*E*) Number of adherent neutrophils and transmigrated neutrophils and rolling velocity in sham-operated mice and ischemic mice treated with vehicle or MLN4924 12 h after stroke ($n = 6$). (*F*) Quantification of Ly6G$^+$ neutrophils at 6, 12, 24, and 48 h ($n = 8$). HPF, high-power field. (*G* and *H*) Representative Western blot and quantification of the amount of neutrophils in the ischemic brain in mice treated with vehicle or MLN4924 at 24 h ($n = 8$). (*I*) Quantification of MPO activity at 24 h ($n = 8$). (*J*–*M*) Relative gene expression of CXCL1, CX3CL1, CCL2, and CCR1 in the ischemic brains of mice at 24 h ($n = 8$). (*N*–*P*) Quantification of proinflammatory cytokines IL-6, IL-1β, and TNF-α by enzyme-linked immunoassay (ELISA) at 24 h ($n = 8$). (*Q* and *R*) Quantification of the number of activated microglia cells and monocytes/macrophages in the ischemic brains of mice at 24 h ($n = 8$). (*S* and *T*) Representative images and quantification of DHE staining reflected the ROS levels in the brains of mice at 24 h ($n = 8$). (Scale bar, 40 μm.) Data were analyzed using one-way ANOVA followed by Bonferroni multiple comparison test. Values are mean ± SD. *$P < 0.05$. NS, not significant.

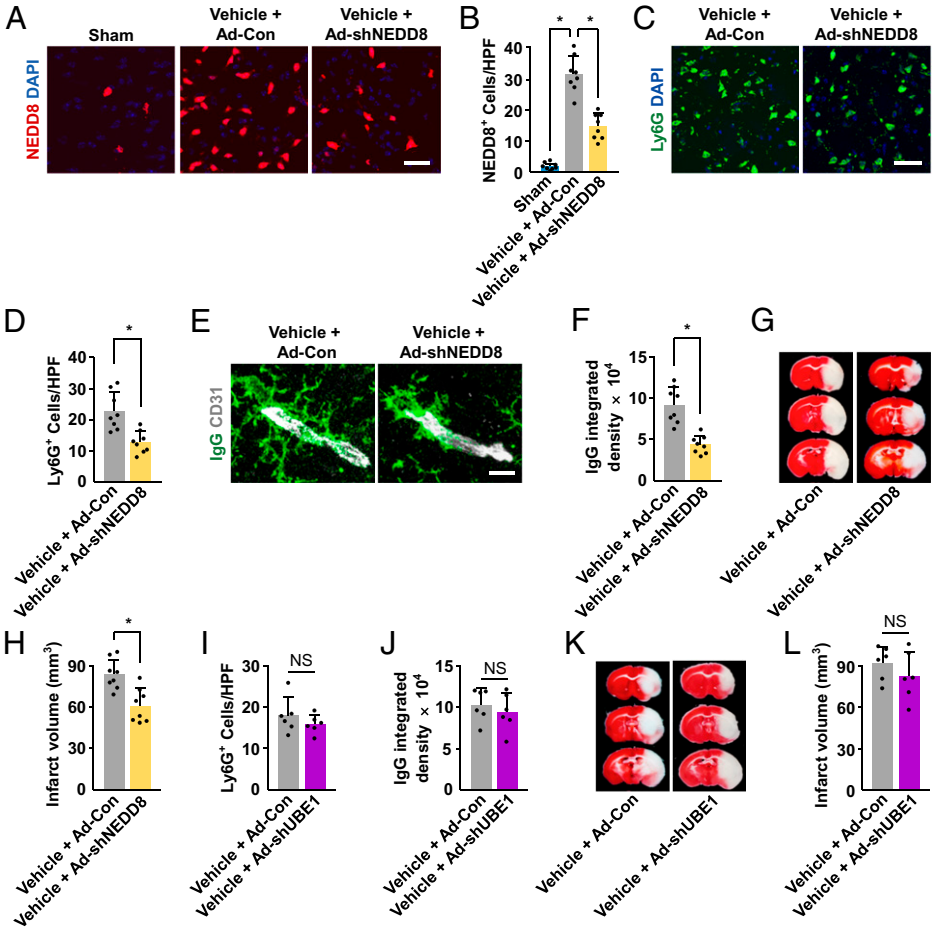

Fig. 5. Effects of NEDD8 or UBE1 silencing on neutrophil infiltration, BBB permeability, and ischemic cerebral injury. (*A* and *B*) Representative NEDD8 immunostaining and quantification of neddylation levels in sham-operated mice and ischemic mice treated with control adenovirus (Ad-Con) or NEDD8 shRNA (Ad-shNEDD8) 24 h following stroke ($n = 8$). HPF, high-power field. (Scale bar, 30 μm.) (*C* and *D*) Representative images and quantification of Ly6G$^+$ neutrophils ($n = 8$). (Scale bar, 30 μm.) (*E* and *F*) Representative images and quantitation of IgG extravascular deposits (green) ($n = 8$). Capillaries were stained with CD31 (white). (Scale bar, 10 μm.) (*G*) Representative photographs of TTC stained coronal brain sections showing cerebral infarct in mice treated with control adenovirus (Ad-Con) or NEDD8 shRNA (Ad-shNEDD8). (*H*) Quantitation of infarct volumes for each group ($n = 8$). (*I*) Quantification of Ly6G$^+$ neutrophils in mice treated with control adenovirus (Ad-Con) or UBE1 shRNA (Ad-shUBE1) 24 h following stroke ($n = 6$). (*J*) Quantitation of IgG extravascular deposits (green) ($n = 6$). Capillaries were stained with CD31 (white). (*K*) Representative photographs of TTC stained coronal brain sections showing cerebral infarct in mice treated with control adenovirus (Ad-Con) or UBE1 shRNA (Ad-shUBE1). (*L*) Quantitation of infarct volumes for each group ($n = 6$). Data were analyzed using unpaired Student's *t* test or one-way ANOVA followed by Bonferroni multiple comparison test. Values are mean ± SD. $^*P < 0.05$. NS, not significant.

further confirmed a significant reduction in neutrophil influx into MLN4924-treated murine brain (Fig. 4*I*). Together, these data suggest that MLN4924 controls both the intravascular adhesion and intraparenchymal migration of neutrophils.

In line with these findings, we found that the mRNA expression levels of neutrophil chemotactic chemokines and chemokine receptor, including CXCL1, CX3CL1, CCL2, and CCR1 (23–26), were significantly lower in MLN4924-treated mice than in controls (Fig. 4 *J*–*M*), suggesting that the reduced accumulation of neutrophils in MLN4924-treated mice may cause by decreased recruitment. In addition, proinflammatory cytokine concentrations of IL-6, IL-1β, and TNFα were also reduced in mice treated with MLN4924 (Fig. 4 *N*–*P*).

Previous studies have shown that depletion of neutrophils after brain injury reduced microglia and macrophage activation (27). In the present study, we observed that treatment with MLN4924 significantly reduced the number of activated microglia cells (Fig. 4*Q* and *SI Appendix*, Fig. S3*B*) in the ischemic cortex. However, MLN4924 did not significantly reduce the infiltration of monocytes/macrophages (Fig. 4*R* and *SI Appendix*, Fig. S3*C*).

ROS are produced during ischemia and reperfusion injury that may contribute to damage the BBB (28). To examine the impact of MLN4924 on the production of ROS, brain sections were stained with dihydroethidium (DHE) and the generation of ROS was analyzed by DHE fluorescence. This analysis showed that treatment with MLN4924 attenuated ROS production compared with phosphate-buffered saline–treated mice at 24 h after stroke (Fig. 4 *S* and *T*), which is consistent with a recent finding reporting that MLN4924 reduced ROS production in a mouse model of diet-induced nonalcoholic fatty liver disease (29).

To further establish the role of neddylation pathway in ischemic stroke, we silenced NEDD8 by adenoviral shRNA injection. Immunohistochemistry analyses with the antibody that recognizes NEDD8-conjugated proteins indicated a marked decrease in the levels of NEDD8 neddylation in the ischemic brain (Fig. 5 *A* and *B*). Moreover, we observed a significant decrease in neutrophil recruitment (Fig. 5 *C* and *D*), leakage of IgG (Fig. 5 *E* and *F*), and infarct volume (Fig. 5 *G* and *H*) in mice subjected to NEDD8 shRNA treatment compared with mice treated with control shRNA. These data suggest that neddylation inhibition in our mouse stroke models may not be

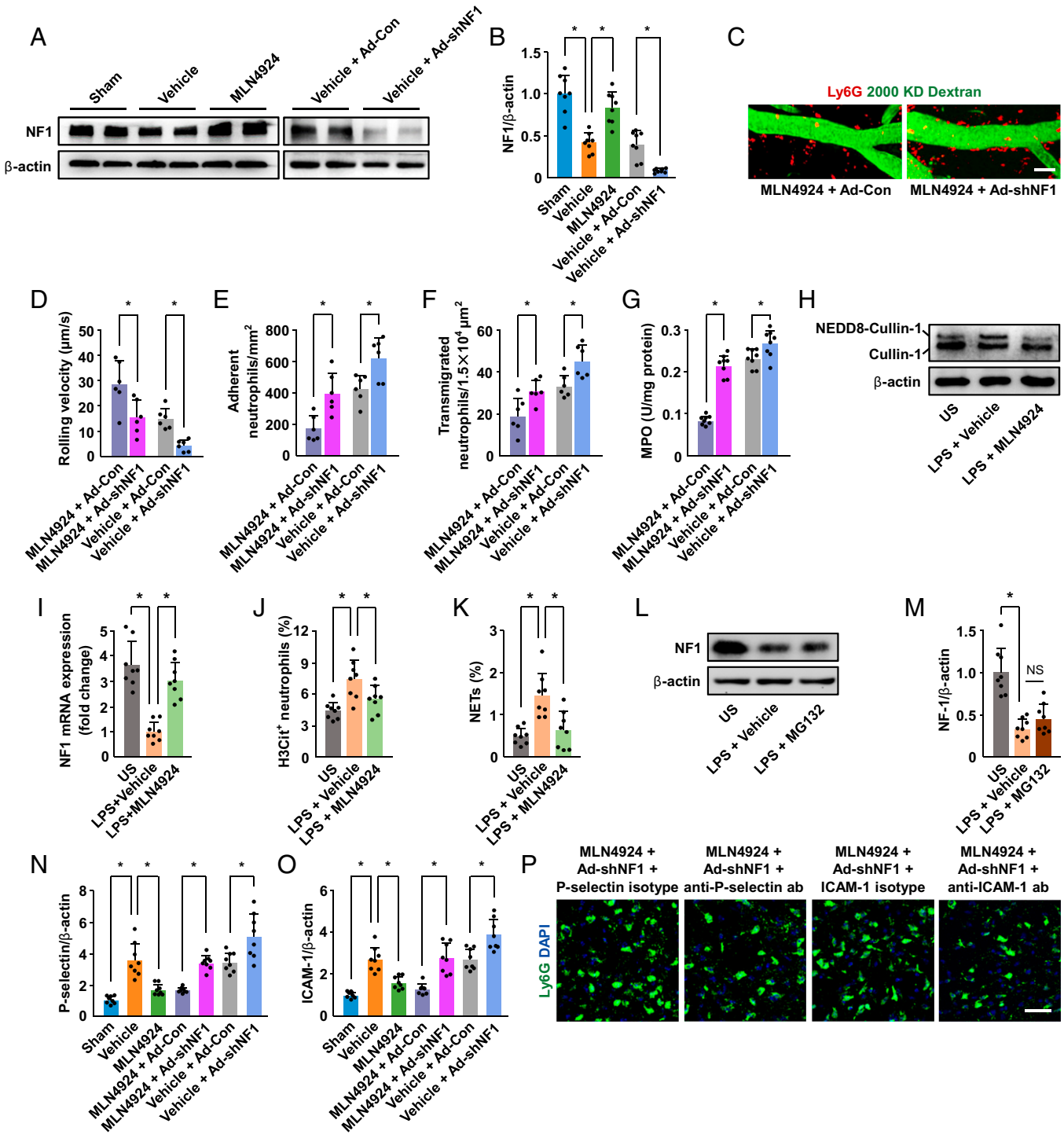

Fig. 6. NF1 silencing abolishes MLN4924-dependent inhibition of neutrophil infiltration. (*A* and *B*) Representative immunoblots and quantification of NF1 levels in the ipsilateral hemisphere in sham-operated mice and ischemic mice treated with vehicle, MLN4924, control adenovirus (Ad-Con), or NF1 shRNA (Ad-shNF1) ($n = 8$). (*C*) Representative in vivo multiphoton microscopic images of rolling and adherent neutrophils (red) inside the blood vessels (green) and of infiltrated neutrophils into the brain parenchyma. (Scale bar, 40 μm.) (*D*–*F*) Rolling velocities and number of adherent neutrophils and transmigrated neutrophils after injection of MLN4924 + control adenovirus (Ad-Con), MLN4924 + NF1 shRNA (Ad-shNF1), control adenovirus, or NF1 shRNA ($n = 6$). (*G*) Quantification of MPO activity in the ischemic brains of mice ($n = 8$). (*H*) Inhibition of cullin-1 neddylation by MLN4924. Immunoblotting of lysates from bone marrow neutrophils isolated from ischemic mice. Neutrophils were incubated with LPS together with vehicle or MLN4924 for 2.5 h. US: neutrophils were incubated without LPS. (*I*) NF1 mRNA expression was measured by quantitative real-time PCR in isolated neutrophils ($n = 8$). (*J* and *K*) Quantification of the percentage of H3Cit-positive neutrophils and NETs in isolated neutrophils ($n = 8$). (*L*) Representative immunoblots of NF1 expression in isolated neutrophils treated with LPS together with vehicle or the proteasome inhibitor MG132 compared with neutrophils incubated without LPS (US). (*M*) Quantitation of NF1 expression for each group ($n = 8$). (*N* and *O*) Quantification of P-selectin and ICAM-1 levels in isolated brain microvessels in sham-operated mice and ischemic mice treated with vehicle, MLN4924, MLN4924 + control adenovirus (Ad-Con), MLN4924 + NF1 shRNA (Ad-shNF1), control adenovirus, or NF1 shRNA ($n = 8$). (*P*) Representative images of Ly6G$^+$ neutrophils. (Scale bar, 30 μm.) Data were analyzed using unpaired Student's *t* test or one-way ANOVA followed by Bonferroni multiple comparison test. Values are mean ± SD. *$P < 0.05$. NS, not significant.

associated with side effects. We next addressed the roles of the ubiquitin E1 enzyme UBE1 silencing after experimental stroke. Our results showed that UBE1 silencing (Fig. 2 *C* and *D*) failed to affect neutrophil recruitment (Fig. 5*I* and *SI Appendix*, Fig. S4*A*), perivascular IgG deposits (Fig. 5*J* and *SI Appendix*, Fig. S4*B*), and infarct volume (Fig. 5 *K* and *L*).

MLN4924 Reduces Neutrophil Infiltration via NF1-Mediated Inhibition of Endothelial P-selectin and ICAM-1 Expression. NF1, a tumor suppressor, is a key substrate of CRL (30). NF1 loss is associated with inflammation and vascular disease (31). We tested the hypothesis that NF1 is critical for MLN4924-mediated inhibition of neutrophil trafficking. Western blot analysis showed that ischemic stroke significantly reduced NF1 expression compared with the sham-operated group (Fig. 6 *A* and *B*). In contrast, injection of MLN4924 preserved the loss of NF1 caused by ischemia. We then hypothesized that NF1 silencing by adenoviral shRNA administration could abolish the inhibitory effect of MLN4924 on neutrophil infiltration. Treatment with NF1 shRNA effectively reduced NF1 expression in the ischemic mice and blocked MLN4924-induced accumulation of NF1 (Fig. 6 *A* and *B* and *SI Appendix*, Fig. S5 *A* and *B*). In vivo multiphoton microscopy indicated that NF1 silencing decreased rolling velocity and increased neutrophil adhesion and transmigration in ischemic mice treated with vehicle or MLN4924 at 12 h after stroke (Fig. 6 *C–F* and *SI Appendix*, Fig. S5*C*). At 24 h, we observed that injection of NF1 shRNA into vehicle-treated or MLN4924-treated mice caused a significant increase in MPO activity (Fig. 6*G*). The MLN4924-mediated decrease in proinflammatory cytokines was also reversed by NF1 silencing (*SI Appendix*, Fig. S5 *D–F*). Injection of NF1 shRNA moderately increased proinflammatory cytokine concentrations of IL-6 and markedly increased IL-1β and TNFα compared with control shRNA treatment.

We then isolated neutrophils from the bone marrow of ischemic mice and incubated them with lipopolysaccharide (LPS). Consistent with previous studies showing that LPS-activated macrophages have increased neddylation activity (12), we observed an increase in neddylated Cullin1 in LPS-treated neutrophils (Fig. 6*H* and *SI Appendix*, Fig. S6*A*). Treatment with MLN4924 reduced cullin-1 neddylation and resulted in a significant increase in NF1 mRNA and protein levels in LPS-treated neutrophils (Fig. 6*I* and *SI Appendix*, Fig. S6 *B* and *C*); this was accompanied by attenuated H3Cit-positive neutrophils and neutrophil extracellular trap formation (Fig. 6 *J* and *K* and *SI Appendix*, Fig. S6*D*). We further studied whether proteasome-mediated protein degradation regulates NF1 expression in neutrophils after LPS stimulation. We found that treatment with the proteasome inhibitor MG132 did not prevent the reduction of NF1 expression in neutrophils upon LPS stimulation (Fig. 6 *L* and *M*), confirming previous results (32). However, NF1 was also reported to be accumulated by the proteasome inhibitors (33). Further study would be important to address the relationship between NF1 and the proteasome.

Extravasation of neutrophils during inflammation is mediated through interactions between adhesion molecules on endothelium and neutrophils (34). We hypothesized that NF1 loss may increase neutrophil extravasation in MLN4924-treated mice by regulating adhesion molecule expression on endothelia cells. Indeed, immunoblotting of isolated brain microvessels showed that the expression of P-selectin and ICAM-1 was significantly reduced in MLN4924-treated mice, whereas this reduction was reversed by NF1 silencing (Fig. 6 *N* and *O* and *SI Appendix*, Fig. S7 *A* and *B*). Injection of NF1 shRNA alone increased the expression of P-selectin and ICAM-1 in ischemic mice treated with vehicle. In addition, MLN4924 treatment did not change the expression of vascular cell adhesion molecule-1 (*SI Appendix*, Fig. S7 *C* and *D*). When using blocking antibodies against P-selectin or using anti-ICAM-1 antibodies, we observed a significant reduction in the numbers of neutrophils in the ischemic brain of mice treated with MLN4924 and NF1 shRNA (Fig. 6*P* and *SI Appendix*, Fig. S7*E*).

NF1 Mediates MLN4924-Afforded BBB Protection via Activation of PKCδ Signals. We next studied the role of NF1 inhibition by shRNA silencing on the protection of BBB with MLN4924 treatment. We observed that NF1 silencing increased BBB permeability (Fig. 7 *A* and *B*) and extravascular accumulation of serum IgG (Fig. 7*C* and *SI Appendix*, Fig. S8*A*) in mice treated with MLN4924; this was accompanied by extended infarct volume (Fig. 7 *D* and *E*) and exacerbated neurological functions (Fig. 7 *F* and *G*). NF1 silencing alone exacerbated BBB disruption, increased infarct volume, and moderately worsened neurological deficits.

As NF1 was reported to regulate PKCδ activity (35) and PKCδ can be activated by ischemia (36), we next studied whether NF1 silencing abolished the protective effect of MLN4924 against BBB damage through PKCδ. Western blot analysis of isolated brain microvessels showed that ischemia-induced phosphorylation of PKCδ was inhibited by MLN4924 treatment, and these effects were reversed by silencing NF1 (Fig. 7 *H* and *I*). Similarly, NF1 silencing efficiently reversed MLN4924-mediated inactivation of MARCKS protein (Fig. 7 *J* and *K* and *SI Appendix*, Fig. S8*B*), a well-recognized substrate for PKC (37). Because MARCKS is a CaM-binding protein (38), we further studied the effects of MLN4924 treatment and NF1 silencing on the CaM-dependent phosphorylation of MLC (pMLC), which has been implicated in endothelial barrier integrity (39). Isolated microvessels from the ischemic brain of MLN4924-treated mice exhibited decreased pMLC compared with vehicle-treated mice (Fig. 7*L* and *SI Appendix*, Fig. S8*C*). However, the decrease in pMLC caused by MLN4924 treatment was abolished by silencing NF1. Injection of NF1 shRNA increased phosphorylation of PKCδ and moderately increased phosphorylation of MARCKS (pMARCKS) and pMLC in ischemic mice. We then injected the PKCδ inhibitor rottlerin in mice subjected to ischemia and coadministration of MLN4924 with NF1 shRNA. Rottlerin substantially reduced NF1 silencing-mediated increase in BBB permeability in MLN4924-treated mice (Fig. 7 *M* and *N*). Together, these data indicate that NF1 silencing blunted MLN4924-provided BBB protection by inducing PKCδ activation.

Discussion

In this study, we found that neddylation was up-regulated in the brain and active in intravascular and intraparenchymal neutrophils after transient focal ischemia in mice. We demonstrated that inhibition of neddylation by the NAE inhibitor MLN4924 improved stroke outcomes by reducing neutrophil infiltration, attenuating BBB damage and infarct volume and improving neurological functions. Furthermore, we show that MLN4924 reduced both neutrophil extravasation and BBB breakdown through attenuation of NEDD8 conjugation to cullin-1, and our data suggest that this is the result of a marked up-regulation of the NF1 signals.

Neutrophils are the first line of innate immune defense against invading pathogens, but they also contribute to endothelial damage and tissue destruction by releasing ROS, proteases, and proinflammatory mediators (3, 40). Our data show expression of vascular adhesion molecules and the accumulation of NEDD8+ neutrophils in the ischemic brain after stroke, suggesting that NEDD8-mediated neutrophil trafficking may cause BBB damage and inflammation. Inhibiting neddylation using a small molecule inhibitor MLN4924 reduced neutrophil infiltration and proinflammatory cytokine production. MLN4924 was shown to cause accumulation of a multitude of different proteins

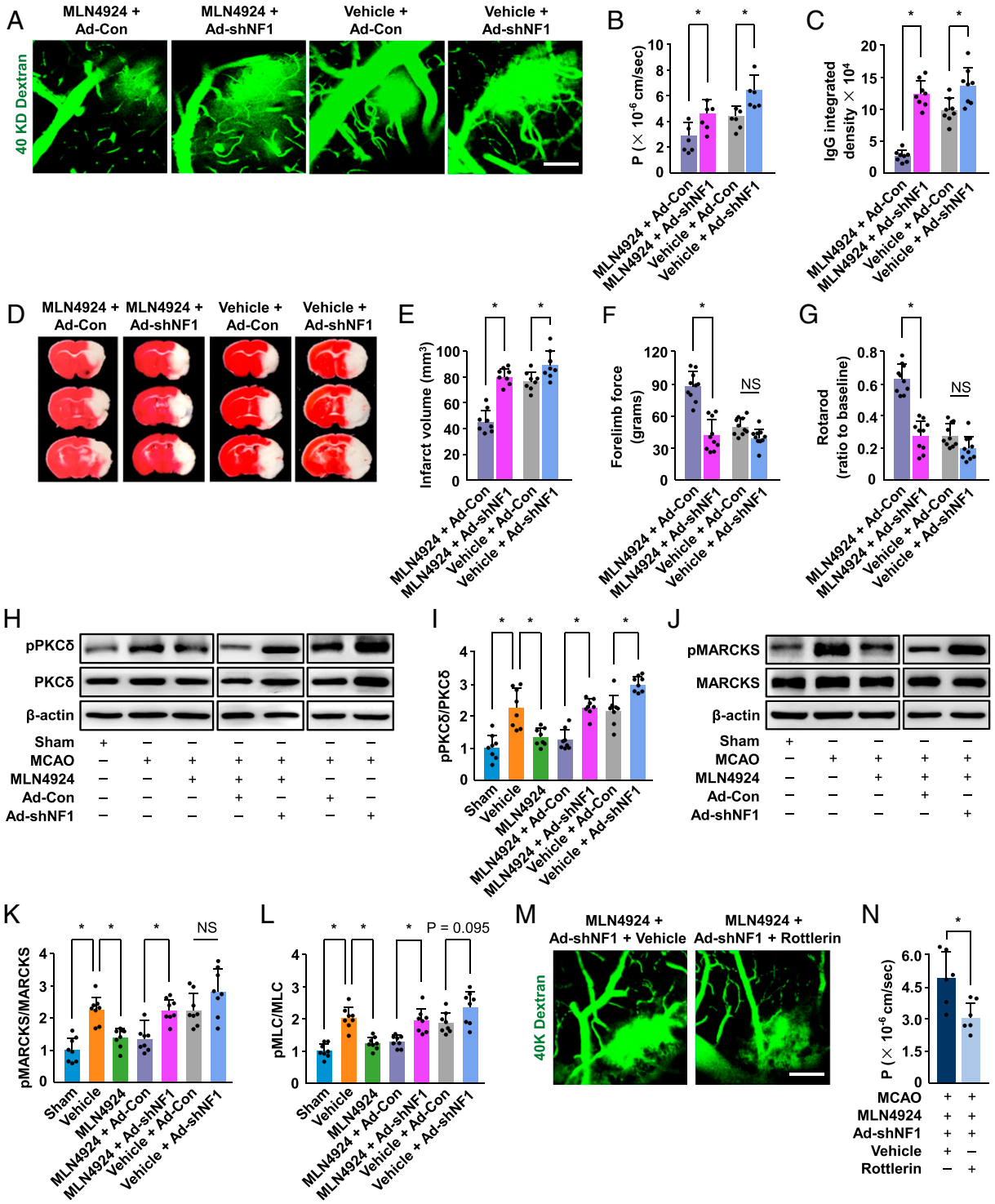

Fig. 7. NF1 silencing blocks MLN4924-afforded BBB protection. (*A*) Representative in vivo multiphoton microscopic images of intravenously injected FITC-dextran leakage from cortical vessels in ischemic mice treated with MLN4924 + control adenovirus (Ad-Con), MLN4924 + NF1 shRNA (Ad-shNF1), control adenovirus, or NF1 shRNA 24 h after stroke. (Scale bar, 100 μm.) (*B*) Quantification of the permeability (P) product of FITC-dextran for each group ($n = 6$). (*C*) Quantification of IgG extravascular deposits ($n = 8$). (*D*) Representative photographs of TTC stained coronal brain sections showing cerebral infarct in mice treated with MLN4924 + control adenovirus (Ad-Con), MLN4924 + NF1 shRNA (Ad-shNF1), control adenovirus, or NF1 shRNA at 24 h. (*E*) Quantitation of infarct volumes for each group ($n = 8$). (*F* and *G*) NF1 silencing worsened neurological outcomes in MLN4924-treated mice ($n = 10$). (*H* and *I*) Representative immunoblots and quantification of pPKCδ levels in isolated brain microvessels in sham-operated mice and ischemic mice treated with vehicle, MLN4924, MLN4924 + control adenovirus (Ad-Con), MLN4924 + NF1 shRNA (Ad-shNF1), control adenovirus, or NF1 shRNA ($n = 8$). (*J* and *K*) Representative immunoblots and quantification of pMARCKS levels in isolated brain microvessels ($n = 8$). (*L*) Quantification of pMLC levels in isolated brain microvessels ($n = 8$). (*M*) Representative in vivo multiphoton microscopic images of intravenously injected FITC-dextran leakage from cortical vessels in MLN4924-treated mice after injection of vehicle or the PKCδ inhibitor rottlerin together with NF1 shRNA (Ad-shNF1). (Scale bar, 100 μm.) (*N*) Quantification of the permeability (P) product of FITC-dextran for each group ($n = 6$). Data were analyzed using unpaired Student's *t* test or one-way ANOVA followed by Bonferroni multiple comparison test. Values are mean ± SD. $^*P < 0.05$. NS, not significant.

by inactivating CRL (41). In this study, we found that MLN4924 significantly increased the accumulation of NF1, a CRL substrate, whereas NF1 silencing by adenoviral shRNA administration induced the expression of P-selectin and ICAM-1 in brain microvessels to increase neutrophil extravasation in MLN4924-treated mice, suggesting that the anti-inflammatory effect of MLN4924 may involve NF1. Importantly, we show here that NF1 silencing-induced increase in neutrophil infiltration in MLN4924-treated mice could be rescued by either blocking antibodies against P-selectin or anti-ICAM-1 antibodies, suggesting the need of a specific interaction between activated neutrophils and injured endothelial cells for induction of neutrophil transmigration.

Inflammation in cerebral vessels contributes to BBB disruption (42), and high BBB permeability correlates with infarction growth (43) and poor clinical prognosis after stroke (44, 45). The present study demonstrated that MLN4924 treatment preserved BBB integrity and thereby reduced BBB permeability after cerebral ischemia. These BBB-protective effects of MLN4924 were accompanied by reduced brain infarctions and less severe neurologic deficits. Furthermore, we show that MLN4924-offered protection against BBB breakdown is depended on its action on NF1. We then attempted to provide information regarding the signaling mechanisms by which NF1 mediated the BBB protection of MLN4924. Our data indicated a robust down-regulation of ischemia-induced activation of PKCδ-MARCKS-MLC pathway upon MLN4924 treatment, and silencing NF1 promoted the activation of PKCδ pathway again and blocked MLN4924-afforded BBB protection. However, in addition to NF1-mediated inactivation of PKCδ pathway, multiple other CRL substrates may also contribute to the effects of MLN4924.

In summary, our study shows a crucial role for protein neddylation in regulating cerebral ischemia. Because of its impressive anticancer efficacy, MLN4924 is currently in phase I/II clinical trials for the treatment of several cancers (46). Our data demonstrated that the neddylation inhibitor MLN4924 protected the brain against ischemic injury by attenuating neutrophil extravasation into brain and maintaining BBB integrity. We conclude that MLN4924 could represent a therapeutic option for ischemic stroke.

Materials and Methods

Detailed descriptions are provided in *SI Appendix*.

Animal Stroke Model. Male C57BL/6 mice (Shanghai SLAC Laboratory Animal Co. Ltd.), 8 to 10 wk old, were used in this study. All protocols for these studies were approved by the Animal Care and Use Committee of the Shanghai Medical College of Fudan University according to NIH Guidelines. Mice were anesthetized with 1 to 1.5% isoflurane in 30% oxygen and 70% nitrous oxide. Focal cerebral ischemia was induced by occlusion of the right MCA for 60 min with a siliconized filament (47).

Cranial Window Surgery and Multiphoton Microscopy. Cranial windows were prepared as we previously described (48, 49). Mice were anesthetized with 1 to 1.5% isoflurane in 30% oxygen and 70% nitrous oxide. Body temperature was maintained at 37 ± 0.5 °C during surgery. After fixation in a stereotaxic head holder, a craniotomy (5 mm diameter) was created above the right somatosensory cortex (centered 2.5 mm lateral and 2.5 mm posterior to the bregma) using a high-speed micro drill. The window was closed with a sterile cover glass. For multiphoton imaging, Olympus FluoView FVMPE-RS upright multiphoton laser-scanning system with an Olympus XL Plan N 25 ×/1.05 WMP ∞/0–0.23/FN/18 dipping objective was used. Multiphoton excitation was performed using MAITAI eHPDS-OL and Spectra-Physics InSight DS-OL lasers (Mai Tai, Spectra-Physics). Emitted fluorescence was detected through 495 to 540 nm and 575 to 645 nm bandpass filters.

Statistics. All values are presented as means ± SD. Statistical analysis for multiple comparisons was performed in Prism 7 software using one-way ANOVA followed by Bonferroni multiple comparison test. Differences between the two groups were assessed by unpaired Student's *t* test. A value of $P < 0.05$ was considered statistically significant.

Data Availability. All study data are included in the article and/or supporting information. In addition, the mass spectrometry proteomics data reported in this paper were uploaded in the ProteomeXchange Consortium (50) via the integrated proteome resources platform (iProX) with the dataset identifier PXD029910 (or the iProX with the dataset identifier IPX0003775000).

ACKNOWLEDGMENTS. We are grateful to the Wu Kong platform (https://www.omicsolution.com/wkomics/main/) developed by Shisheng Wang (West China Hospital, Sichuan University) for the relative statistical analysis. This work was supported by grants from the National Natural Science Foundation of China (General Program 81671156, 31872777, and 81873744, Key Program 81530034), National Key Research and Development Program Special Items sponsored by the Ministry of Science and Technology of China (2016YFC1300501 and 2016YFC1300502), Shanghai Municipal Science and Technology Major Project (No. 2018SHZDZX01), ZJ Lab, and Shanghai Center for Brain Science and Brain-Inspired Technology.

1. Y. Okada *et al.*, P-selectin and intercellular adhesion molecule-1 expression after focal brain ischemia and reperfusion. *Stroke* **25**, 202–211 (1994).
2. M. Gelderblom *et al.*, Temporal and spatial dynamics of cerebral immune cell accumulation in stroke. *Stroke* **40**, 1849–1857 (2009).
3. M. Scholz, J. Cinatl, M. Schadel-Hopfner, J. Windolf, Neutrophils and the blood-brain barrier dysfunction after trauma. *Med. Res. Rev.* **27**, 401–416 (2007).
4. T. Kamitani, K. Kito, H. P. Nguyen, E. T. Yeh, Characterization of NEDD8, a developmentally down-regulated ubiquitin-like protein. *J. Biol. Chem.* **272**, 28557–28562 (1997).
5. C. Schwechheimer, NEDD8-its role in the regulation of Cullin-RING ligases. *Curr. Opin. Plant Biol.* **45**, 112–119 (2018).
6. R. Hjerpe, Y. Thomas, T. Kurz, NEDD8 overexpression results in neddylation of ubiquitin substrates by the ubiquitin pathway. *J. Mol. Biol.* **421**, 27–29 (2012).
7. W. J. Errington *et al.*, Adaptor protein self-assembly drives the control of a cullin-RING ubiquitin ligase. *Structure* **20**, 1141–1153 (2012).
8. J. Merlet, J. Burger, J. E. Gomes, L. Pintard, Regulation of cullin-RING E3 ubiquitin-ligases by neddylation and dimerization. *Cell. Mol. Life Sci.* **66**, 1924–1938 (2009).
9. M. El-Mesery, M. A. Anany, S. H. Hazem, M. E. Shaker, The NEDD8-activating enzyme inhibition with MLN4924 sensitizes human cancer cells of different origins to apoptosis and necroptosis. *Arch. Biochem. Biophys.* **691**, 108513 (2020).
10. I. Zubiete-Franco *et al.*, Deregulated neddylation in liver fibrosis. *Hepatology* **65**, 694–709 (2017).
11. K. L. Kuo *et al.*, MLN4924, a novel protein neddylation inhibitor, suppresses proliferation and migration of human urothelial carcinoma: In vitro and in vivo studies. *Cancer Lett.* **363**, 127–136 (2015).
12. F. M. Chang *et al.*, Inhibition of neddylation represses lipopolysaccharide-induced proinflammatory cytokine production in macrophage cells. *J. Biol. Chem.* **287**, 35756–35767 (2012).
13. D. Pandey *et al.*, NEDDylation promotes endothelial dysfunction: A role for HDAC2. *J. Mol. Cell. Cardiol.* **81**, 18–22 (2015).
14. J. E. Brownell *et al.*, Substrate-assisted inhibition of ubiquitin-like protein-activating enzymes: The NEDD8 E1 inhibitor MLN4924 forms a NEDD8-AMP mimetic in situ. *Mol. Cell* **37**, 102–111 (2010).
15. S. Lobato-Gil *et al.*, Proteome-wide identification of NEDD8 modification sites reveals distinct proteomes for canonical and atypical NEDDylation. *Cell Rep.* **34**, 108635 (2021).
16. L. G. Wu, E. Hamid, W. Shin, H. C. Chiang, Exocytosis and endocytosis: Modes, functions, and coupling mechanisms. *Annu. Rev. Physiol.* **76**, 301–331 (2014).
17. M. Curcio, I. L. Salazar, M. Mele, L. M. Canzoniero, C. B. Duarte, Calpains and neuronal damage in the ischemic brain: The swiss knife in synaptic injury. *Prog. Neurobiol.* **143**, 1–35 (2016).
18. K. A. Kim *et al.*, Role of autophagy in endothelial damage and blood-brain barrier disruption in ischemic stroke. *Stroke* **49**, 1571–1579 (2018).
19. W. Yao *et al.*, Glycine exerts dual roles in ischemic injury through distinct mechanisms. *Stroke* **43**, 2212–2220 (2012).
20. E. Y. Zhao, A. Efendizade, L. Cai, Y. Ding, The role of Akt (protein kinase B) and protein kinase C in ischemia-reperfusion injury. *Neurol. Res.* **38**, 301–308 (2016).
21. E. Sidorov *et al.*, Potential metabolite biomarkers for acute versus chronic stage of ischemic stroke: A pilot study. *J. Stroke Cerebrovasc. Dis.* **29**, 104618 (2020).
22. D. Knowland *et al.*, Stepwise recruitment of transcellular and paracellular pathways underlies blood-brain barrier breakdown in stroke. *Neuron* **82**, 603–617 (2014).
23. S. Paudel *et al.*, CXCL1 regulates neutrophil homeostasis in pneumonia-derived sepsis caused by Streptococcus pneumoniae serotype 3. *Blood* **133**, 1335–1345 (2019).
24. R. Brauer *et al.*, MMP-19 deficiency causes aggravation of colitis due to defects in innate immune cell function. *Mucosal Immunol.* **9**, 974–985 (2016).

25. C. Rouault *et al.*, Roles of chemokine ligand-2 (CXCL2) and neutrophils in influencing endothelial cell function and inflammation of human adipose tissue. *Endocrinology* **154**, 1069–1079 (2013).
26. Y. Kiyasu *et al.*, Disruption of CCR1-mediated myeloid cell accumulation suppresses colorectal cancer progression in mice. *Cancer Lett.* **487**, 53–62 (2020).
27. E. Kenne, A. Erlandsson, L. Lindbom, L. Hillered, F. Clausen, Neutrophil depletion reduces edema formation and tissue loss following traumatic brain injury in mice. *J. Neuroinflammation* **9**, 17 (2012).
28. A. Chamorro, U. Dirnagl, X. Urra, A. M. Planas, Neuroprotection in acute stroke: Targeting excitotoxicity, oxidative and nitrosative stress, and inflammation. *Lancet Neurol.* **15**, 869–881 (2016).
29. M. Serrano-Macia *et al.*, Neddylation inhibition ameliorates steatosis in NAFLD by boosting hepatic fatty acid oxidation via the DEPTOR-mTOR axis. *Mol. Metab.* **53**, 101275 (2021).
30. A. Upadhyay *et al.*, E3 ubiquitin ligases neurobiological mechanisms: Development to Degeneration. *Front. Mol. Neurosci.* **10**, 151 (2017).
31. E. A. Lasater *et al.*, Genetic and cellular evidence of vascular inflammation in neurofibromin-deficient mice and humans. *J. Clin. Invest.* **120**, 859–870 (2010).
32. H. F. Wang *et al.*, Valosin-containing protein and neurofibromin interact to regulate dendritic spine density. *J. Clin. Invest.* **121**, 4820–4837 (2011).
33. Y. S. Green *et al.*, Hypoxia-associated factor (HAF) mediates neurofibromin ubiquitination and degradation leading to ras-ERK pathway activation in hypoxia. *Mol. Cancer Res.* **17**, 1220–1232 (2019).
34. C. Justicia *et al.*, Uric acid is protective after cerebral ischemia/reperfusion in hyperglycemic mice. *Transl. Stroke Res.* **8**, 294–305 (2017).
35. P. Ghoshal *et al.*, Loss of GTPase activating protein neurofibromin stimulates paracrine cell communication via macropinocytosis. *Redox Biol.* **27**, 101224 (2019).
36. A. Hafeez *et al.*, Reduced apoptosis by ethanol and its association with PKC-delta and Akt Signaling in Ischemic Stroke. *Aging Dis.* **5**, 366–372 (2014).
37. P. J. Blackshear, The MARCKS family of cellular protein kinase C substrates. *J. Biol. Chem.* **268**, 1501–1504 (1993).
38. J. H. Hartwig *et al.*, MARCKS is an actin filament crosslinking protein regulated by protein kinase C and calcium-calmodulin. *Nature* **356**, 618–622 (1992).
39. C. R. Kuhlmann *et al.*, Inhibition of the myosin light chain kinase prevents hypoxia-induced blood-brain barrier disruption. *J. Neurochem.* **102**, 501–507 (2007).
40. N. Sorvillo, D. Cherpokova, K. Martinod, D. D. Wagner, Extracellular DNA NET-works with dire consequences for Health. *Circ. Res.* **125**, 470–488 (2019).
41. J. J. Shah *et al.*, Phase I study of the novel investigational NEDD8-activating enzyme inhibitor pevonedistat (MLN4924) in patients with relapsed/refractory multiple myeloma or lymphoma. *Clin. Cancer Res.* **22**, 34–43 (2016).
42. B. W. McColl, N. J. Rothwell, S. M. Allan, Systemic inflammation alters the kinetics of cerebrovascular tight junction disruption after experimental stroke in mice. *J. Neurosci.* **28**, 9451–9462 (2008).
43. R. L. Zhang *et al.*, Synergistic effect of an endothelin type A receptor antagonist, S-0139, with rtPA on the neuroprotection after embolic stroke. *Stroke* **39**, 2830–2836 (2008).
44. S. Warach, L. L. Latour, Evidence of reperfusion injury, exacerbated by thrombolytic therapy, in human focal brain ischemia using a novel imaging marker of early blood-brain barrier disruption. *Stroke* **35**, 2659–2661 (2004).
45. R. Khatri, A. M. McKinney, B. Swenson, V. Janardhan, Blood-brain barrier, reperfusion injury, and hemorrhagic transformation in acute ischemic stroke. *Neurology* **79**, S52–S57 (2012).
46. S. Han *et al.*, The protein neddylation inhibitor MLN4924 suppresses patient-derived glioblastoma cells via inhibition of ERK and AKT signaling. *Cancers (Basel)* **11**, 1849 (2019).
47. L. Wang *et al.*, Recombinant ADAMTS13 reduces tissue plasminogen activator-induced hemorrhage after stroke in mice. *Ann. Neurol.* **73**, 189–198 (2013).
48. H. Xu *et al.*, ADAMTS13 controls vascular remodeling by modifying VWF reactivity during stroke recovery. *Blood* **130**, 11–22 (2017).
49. L. Kang *et al.*, Neutrophil extracellular traps released by neutrophils impair revascularization and vascular remodeling after stroke. *Nat. Commun.* **11**, 2488 (2020).
50. E. W. Deutsch *et al.*, The ProteomeXchange consortium in 2020: Enabling 'big data' approaches in proteomics. *Nucleic Acids Res.* **48**, D1145–D1152 (2020).